



Bidirectional mode-division multiplexers with antireflection gratings

Hossam M. H. Shalaby^{1,2}

¹Electrical Engineering Department, Faculty of Engineering, Alexandria University, Alexandria 21544, Egypt

²Department of Electronics and Communications Engineering, Egypt-Japan University of Science and Technology (E-JUST), Alexandria 21934, Egypt (shalaby@ieee.org)

Received 8 August 2017; revised 25 November 2017; accepted 14 December 2017; posted 18 December 2017 (Doc. ID 304401); published 18 January 2018

A bidirectional mode-division multiplexer (BMDM) with antireflection gratings is designed, and its performance in terms of S -parameters is presented. A BMDM can (de)multiplex three modes with only two waveguides and a Bragg grating. The impact of return losses on the performance of BMDMs is studied and antireflection gratings are designed to reduce their effects. A theoretical analysis of the proposed (de)multiplexer is developed based on the perturbative coupled-mode theory. Analytical expressions for the coupled-mode equations of the proposed device are obtained, taking into account the effects of return losses. Both duty cycle and teeth depths of the antireflection gratings are determined based on optimizing a cost function. In addition, FDTD simulation of the proposed device is performed, and its S -parameters are obtained and studied. © 2018 Optical Society of America

OCIS codes: (130.0130) Integrated optics; (130.3120) Integrated optics devices; (310.2790) Guided waves.

<https://doi.org/10.1364/AO.57.000476>

1. INTRODUCTION

Space-division multiplexing techniques are promising candidates to meet increasingly required demand of high transmission rates in optical fibers and data centers [1–4]. One important scheme to achieve space-division multiplexing is to use multiple modes in few-mode fibers or multimode waveguides. Furthermore, hybrid mode- and wavelength-division multiplexing techniques can be used simultaneously to achieve petabit/s transmission rates [5,6].

Accordingly, mode-division multiplexers (MDMs) are getting increasing interest in recent years [3–28]. MDMs based on asymmetrical directional couplers have been proposed and studied by many authors, e.g. [8,9]. MDMs based on tapered asymmetrical grating-assisted directional couplers have been studied in [10,21]. Microring-based on-chip WDM-compatible mode-division multiplexing has been shown in [14]. Design and fabrication of a two-mode SOI ring resonator for MDM systems have been presented in [16]. An on-chip simultaneous MDM and a wavelength-division multiplexer using a tapered directional coupler and a multimode interference waveguide have been proposed in [24]. An ultra-broadband 16-channel mode-division (de)multiplexer utilizing densely packed bent waveguide arrays has been demonstrated in [28]. An on-chip reconfigurable optical add-drop

multiplexer for mode- and wavelength-division multiplexing has been proposed in [6].

In [25], we have proposed a compact mode-division (de)multiplexer, called a bidirectional MDM (BMDM), which can (de)multiplex three modes with only two waveguides and a Bragg grating. The input waveguide is multimode, while the output waveguide is single mode. Both first- and second-order modes of the input waveguide are coupled to the output waveguide, propagating at opposite directions, while the fundamental mode is kept in the main input waveguide. Simulations have shown that the device is very compact in size, about 17 μm . Two examples have been presented in [25], specifically, a slab waveguide with three TE modes (TE_0 , TE_1 , and TE_2) as well as a slab waveguide with two TE modes and one TM mode (TE_0 , TM_1 , and TE_2). It turned out that in the former case both TE_1 and TE_2 modes have high insertion losses due to contradirectional coupling between them in the input waveguide. These losses are reduced in the latter case. However, owing to some back reflections in the main waveguide, the insertion losses of the device are still somewhat high, about -0.57 dB for fundamental TE_0 mode, while it is about -2.85 dB and -3.8 dB for TM_1 and TE_2 modes, respectively. Furthermore, the loss in TM_1 mode limits the device bandwidth to about 20 nm. In [26], we have extended the concept to strip waveguides. A BMDM based on strip waveguides has been fabricated and tested [29]. In [27], we

have proposed a simple and compact mode-division demultiplexer using a slightly modified rib waveguide. The structure can demultiplex three modes, and has low insertion losses and crosstalks over a wide bandwidth.

Antireflection (AR) design can be used in the waveguides to eliminate the conventional Bragg reflections. This is accomplished by placing two different gratings on each side of the waveguide. If the gratings are phase shifted by 180°, complete cancellation of Bragg back reflections can be achieved. This idea has been adopted in WDM add-drop filters and demultiplexers [30,31].

In this paper, we develop a theoretical analysis of the BMDM when placing antireflection gratings around its outer boundaries. We follow a similar analysis to that in [25], which has been based on the perturbative coupled-mode theory. However, in [25], we have neglected the effect of return losses to simplify the analysis and have some insight on the concept. The impact of return loss is considered in this paper, and the effect of antireflection gratings is studied as well. Using the developed analytical expressions, we design antireflections gratings that reduce the effect of return losses and increase the bandwidth. In addition, 2D finite-difference time-domain (FDTD) simulation of the proposed BMDM with antireflection gratings is performed for a slab-waveguide coupler under different design parameters, and sets of *S*-parameters are determined. Our results reveal that the BMDM with antireflection gratings can achieve acceptable values of insertion losses, return losses, and crosstalks over a wide bandwidth.

The rest of this paper is organized as follows. The structure of the proposed (de)multiplexer with antireflection gratings is described in Section 2. The theoretical analysis of the device and derivation of corresponding coupled-mode equations are given in Section 3. Section 4 is devoted for the solution of the coupled-mode equations and design of antireflection gratings. In Section 5, FDTD simulations of the proposed device are performed under different design parameters, and the resulting set of *S*-parameters is discussed. Our concluding remarks are given in Section 6.

2. STRUCTURE OF BMDM WITH ANTIREFLECTION GRATINGS

Figure 1 shows the structure of the proposed MDM with antireflection gratings (BMDM-AR). The structure is an extension of a traditional BMDM. The widths of the multimode and single-mode guiding layers are *w* and *d*, respectively. The period of

the Bragg grating is Λ and the coupling length is *L*. The gap between the two guiding layers is *r* and the depth of the grating teeth is $t \leq r$. Antireflection gratings at the boundaries of the (de)multiplexer with phase shift of 180° are added to the traditional BMDM. This would reduce the back reflections and increase the operating bandwidth. The depths of the antireflection gratings' teeth at the single-mode and multimode sides are t_d and t_w , respectively. Each of these gratings has a duty cycle of *D*. The refractive indices of the waveguides and claddings are n_1 and n_2 , respectively. A taper at port 2 is used to convert the multimode waveguide to a single mode. The taper length is designed to be

$$\ell_{\text{taper}} \approx \frac{(w - d)/2}{\tan\left(\sin^{-1} \frac{n_{\text{eff}1}}{n_1} - \sin^{-1} \frac{n_2}{n_1}\right)}, \quad (1)$$

where $n_{\text{eff}1}$ is the effective index of the multimode waveguide when excited with TM_1 mode. This taper would let the crosstalk due to TM_1 leak away from the port 2 waveguide.

A. Perturbative Model

Using the perturbation approach, the refractive index of the BMDM-AR structure can be written as

$$\begin{aligned} n^2(x, z) &= n_{\text{multi}}^2(x) + \Delta n_{\text{multi}}^2(x, z) \\ &= n_{\text{single}}^2(x) + \Delta n_{\text{single}}^2(x, z), \end{aligned} \quad (2)$$

where $n_{\text{multi}}(x)$ and $n_{\text{single}}(x)$ are the refractive indices for the unperturbed multimode and single-mode waveguides, respectively. Using Fig. 1, they are given by

$$\begin{aligned} n_{\text{multi}}^2(x) &= \begin{cases} n_1^2; & |x| \leq w/2, \\ n_2^2; & \text{otherwise,} \end{cases} \\ n_{\text{single}}^2(x) &= \begin{cases} n_1^2; & |x - w/2 - r - d/2| \leq d/2, \\ n_2^2; & \text{otherwise.} \end{cases} \end{aligned} \quad (3)$$

Assuming that $L \gg \Lambda$, the periodic dielectric perturbations of the refractive indices can be expanded using Fourier series as

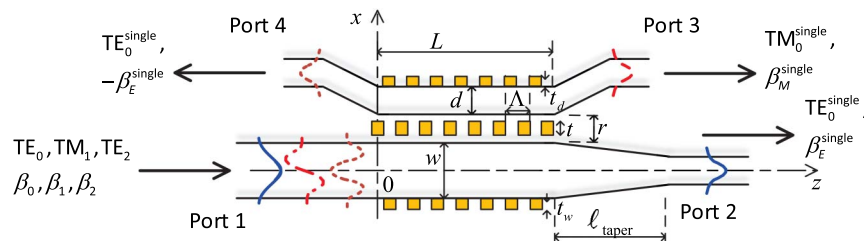


Fig. 1. Structure of a BMDM with antireflection gratings.

$$\Delta n_{\text{multi}}^2(x, z) = \begin{cases} \sum_{\nu=-\infty}^{\infty} b_{\nu} e^{-j\nu(2\pi/\Lambda)z}; & |x - w/2 - r/2| \leq t/2, \\ \sum_{\nu=-\infty}^{\infty} c_{\nu} e^{-j\nu(2\pi/\Lambda)z}; & |x - w/2 - r - d - t_d/2| \leq t_d/2, \\ \sum_{\nu=-\infty}^{\infty} c_{\nu} e^{-j\nu(2\pi/\Lambda)z}; & |x + w/2 + t_w/2| \leq t_w/2, \\ 2b_0; & |x - w/2 - r - d/2| \leq d/2, \\ 0; & \text{otherwise,} \end{cases}$$

$$\Delta n_{\text{single}}^2(x, z) = \begin{cases} \sum_{\nu=-\infty}^{\infty} b_{\nu} e^{-j\nu(2\pi/\Lambda)z}; & |x - w/2 - r/2| \leq t/2, \\ \sum_{\nu=-\infty}^{\infty} c_{\nu} e^{-j\nu(2\pi/\Lambda)z}; & |x - w/2 - r - d - t_d/2| \leq t_d/2, \\ \sum_{\nu=-\infty}^{\infty} c_{\nu} e^{-j\nu(2\pi/\Lambda)z}; & |x + w/2 + t_w/2| \leq t_w/2, \\ 2b_0; & |x| \leq w/2, \\ 0; & \text{otherwise,} \end{cases} \quad (4)$$

where for any $\nu \in \{\dots, -1, 0, 1, \dots\}$ and $\alpha = (3 - 2D)\Lambda/4$,

$$b_{\nu} = \frac{n_1^2 - n_2^2}{2} \text{sinc}(\nu/2), \quad c_{\nu} = (n_1^2 - n_2^2)D \text{sinc}(\nu D) e^{j\nu 2\pi\alpha/\Lambda}. \quad (5)$$

3. THEORETICAL ANALYSIS

In this section, we aim at obtaining analytical expressions for the coupled-mode equations of the proposed device when excited with the first-order TM mode, TM_1 . The analysis is developed based on the perturbative coupled-mode theory, and the expressions are obtained for simple a slab-waveguide coupler. We take into account the effect of return loss, which has been neglected in [25]. The wavelength dependence of the device is addressed by considering mismatching conditions. In our analysis, we focus on TM_1 mode as it has a significant return loss and a small bandwidth.

A. BMDM-AR Fields

The input electric and magnetic fields of the TE and TM modes to the multimode waveguide of the BMDM-AR can be written as

$$E_i^{0,2} = \mathcal{E}_0(x) e^{-j\beta_0 z} + \mathcal{E}_2(x) e^{-j\beta_2 z}, \quad H_i^1 = \mathcal{H}_1(x) e^{-j\beta_1 z}, \quad (6)$$

respectively, where for any $m \in \{0, 2\}$, $\mathcal{E}_m(x)$ is the electric field profile of the m th order TE mode TE_m , $\mathcal{H}_1(x)$ is the magnetic field profile of the first-order TM mode TM_1 , and $\beta_m = 2\pi n_{\text{eff}_m} / \lambda_0$, $m \in \{0, 1, 2\}$, is the corresponding propagation constant. Here, λ_0 is the operating wavelength, and n_{eff_m} is the effective index of mode m at the input waveguide of width w . Specifically, we have the following set of modes: $\mathcal{M} = \{\text{TE}_0, \text{TM}_1, \text{TE}_2\}$. This selection would reduce both the insertion losses and crosstalks [25]. The field profiles are orthogonal, and each mode field is normalized (corresponding to a power flow of one watt per unit width in y direction):

$$\int \mathcal{E}_n^*(x) \mathcal{E}_m(x) dx = \frac{2\omega\mu_0}{\beta_m} \delta_{nm}, \quad n, m \in \{0, 2\},$$

$$\int \frac{1}{n_{\text{multi}}^2(x)} |\mathcal{H}_1(x)|^2 dx = \frac{2\omega\epsilon_0}{\beta_1}, \quad (7)$$

where δ_{nm} is the Kronecker delta, $\mu_0 = 4\pi \times 10^{-7}$ H/m is the permeability of free space, $\epsilon_0 = 8.854 \times 10^{-12}$ F/m is the permittivity of free space, and ω is the angular frequency.

Let $\mathcal{E}_0(x)$ denote the electric field profile of fundamental TE mode $\text{TE}_0^{\text{single}}$ of a single-mode waveguide of width d . In addition, let $\mathcal{H}_0(x)$ denote the magnetic field profile of fundamental TM mode $\text{TM}_0^{\text{single}}$ of the single-mode waveguide. The width d can be selected so that the effective index of mode TM_1 of the multimode waveguide equals that of the fundamental TM mode of the single-mode waveguide, $n_{\text{eff}_1} \approx n_{\text{eff}_M}^{\text{single}}$, where $n_{\text{eff}_M}^{\text{single}}$ is the effective index of $\text{TM}_0^{\text{single}}$ mode. In this case, mode TM_1 will mostly couple codirectionally to $\text{TM}_0^{\text{single}}$. In addition, a grating coupler of period Λ is designed so that mode TE_2 would couple to the contradirectional mode of the single-mode waveguide $\text{TE}_0^{\text{single}}$ with effective index $n_{\text{eff}_E}^{\text{single}}$.

The electric field in the coupling region ($L \geq z \geq 0$) of the BMDM-AR can be written as

$$E_c^{0,2} = A_0^+(z) \mathcal{E}_0(x) e^{-j\beta_0 z} + A_0^-(z) \mathcal{E}_0(x) e^{j\beta_0 z} \\ + A_2^+(z) \mathcal{E}_2(x) e^{-j\beta_2 z} + A_2^-(z) \mathcal{E}_2(x) e^{j\beta_2 z} \\ + B_0^+(z) \mathcal{E}_0(x) e^{-j\beta_E^{\text{single}} z} + B_0^-(z) \mathcal{E}_0(x) e^{j\beta_E^{\text{single}} z}, \\ H_c^1 = A_1^+(z) \mathcal{H}_1(x) e^{-j\beta_1 z} + A_1^-(z) \mathcal{H}_1(x) e^{j\beta_1 z} \\ + C_0^+(z) \mathcal{H}_0(x) e^{-j\beta_M^{\text{single}} z} + C_0^-(z) \mathcal{H}_0(x) e^{j\beta_M^{\text{single}} z}, \quad (8)$$

where $A_m^{\pm}(z)$, $m \in \{0, 1, 2\}$, is a z -dependent complex amplitude of the electric/magnetic field of m th codirectional/contradirectional (+/-) mode of the multimode waveguide, $B_0^{\pm}(z)$ is the complex amplitude of the electric field of fundamental codirectional/contradirectional (+/-) TE mode of the single-mode waveguide, and $C_0^{\pm}(z)$ is the complex amplitude of the magnetic field of fundamental codirectional/contradirectional (+/-) TM mode of the single-mode waveguide. Here, the propagation constants $\beta_E^{\text{single}} = 2\pi n_{\text{eff}_E}^{\text{single}} / \lambda_0$ and $\beta_M^{\text{single}} = 2\pi n_{\text{eff}_M}^{\text{single}} / \lambda_0$.

B. Coupled-Mode Equations

As mentioned earlier, the loss in TM_1 mode in the main source limits the device bandwidth to about 20 nm. Our focus in this and subsequent sections is to optimize the design of the anti-reflection gratings based on this mode only (optimize the worst-case scenario). Of course, a better design is to optimize the system based on the three modes TE_0 , TM_1 , and TE_2 simultaneously. However, this leads to a set of tedious equations with not much improvement than that based on optimizing the worst-case scenario only. Following a similar analysis to that in [25], the coupled-mode equations of TM modes are obtained as in Eq. (9) at the top of next page, where $\Delta\beta_1 = \beta_1(\lambda) - \pi/\Lambda$ and $\Delta\beta_M^{\text{single}} = \beta_M^{\text{single}}(\lambda) - \pi/\Lambda$ with $\beta_1(\lambda)$ and $\beta_M^{\text{single}}(\lambda)$ are the propagation constants of TM_1 and TM_0 modes in both the multimode and single-mode waveguides, respectively, evaluated at wavelength λ . Also, w_{rel} and d_{rel} are relative waveguides widths, given by

$$\begin{aligned}
 \frac{1}{w_{\text{rel}}} \frac{dA_1^+}{dz} &= -j \left[(b_0 \zeta_1 + c_0 \chi_1) A_1^+(z) + (b_0 \kappa_1 + 2b_0 \varsigma_1) C_0^+(z) e^{j(\Delta\beta_1 - \Delta\beta_M^{\text{single}})z} \right. \\
 &\quad \left. + (b_1 \zeta_1 + c_1 \chi_1) A_1^-(z) e^{j2\Delta\beta_1 z} + b_1 \kappa_1 C_0^-(z) e^{j(\Delta\beta_1 + \Delta\beta_M^{\text{single}})z} \right], \\
 \frac{1}{d_{\text{rel}}} \frac{dC_0^+}{dz} &= -j \left[(b_0 \kappa_1^* + 2b_0 \varpi_1) A_1^+(z) e^{-j(\Delta\beta_1 - \Delta\beta_M^{\text{single}})z} + (b_0 t_0 + c_0 \vartheta_0) C_0^+(z) \right. \\
 &\quad \left. + b_1 \kappa_1^* A_1^-(z) e^{j(\Delta\beta_1 + \Delta\beta_M^{\text{single}})z} + (b_1 t_0 + c_1 \vartheta_0) C_0^-(z) e^{j2\Delta\beta_M^{\text{single}} z} \right], \\
 \frac{1}{w_{\text{rel}}} \frac{dA_1^-}{dz} &= j \left[(b_1^* \zeta_1 + c_1^* \chi_1) A_1^+(z) e^{-j2\Delta\beta_1 z} + b_1^* \kappa_1 C_0^+(z) e^{-j(\Delta\beta_1 + \Delta\beta_M^{\text{single}})z} \right. \\
 &\quad \left. + (b_0 \zeta_1 + c_0 \chi_1) A_1^-(z) + (b_0 \kappa_1 + 2b_0 \varsigma_1) C_0^-(z) e^{-j(\Delta\beta_1 - \Delta\beta_M^{\text{single}})z} \right], \\
 \frac{1}{d_{\text{rel}}} \frac{dC_0^-}{dz} &= j \left[b_1^* \kappa_1^* A_1^+(z) e^{-j(\Delta\beta_1 + \Delta\beta_M^{\text{single}})z} + (b_1^* t_0 + c_1^* \vartheta_0) C_0^+(z) e^{-j2\Delta\beta_M^{\text{single}} z} \right. \\
 &\quad \left. + (b_0 \kappa_1^* + 2b_0 \varpi_1) A_1^-(z) e^{j(\Delta\beta_1 - \Delta\beta_M^{\text{single}})z} + (b_0 t_0 + c_0 \vartheta_0) C_0^-(z) \right], \tag{9}
 \end{aligned}$$

$$\begin{aligned}
 w_{\text{rel}} &= \frac{w + Q(\gamma_1, \varrho_1)}{w + R(\gamma_1, \varrho_1)}, \\
 d_{\text{rel}} &= \frac{d + Q(\gamma_{\text{single}}, \varrho_{\text{single}})}{d + R(\gamma_{\text{single}}, \varrho_{\text{single}})}, \tag{10}
 \end{aligned}$$

where the functions $Q(\cdot)$ and $R(\cdot)$ are defined as

$$\begin{aligned}
 Q(\gamma, \varrho) &\stackrel{\text{def}}{=} \frac{2}{\gamma} \left(\frac{n_1}{n_2} \right)^2 \frac{1 + \left(\frac{\gamma}{\varrho} \right)^2}{1 + \left[\left(\frac{n_1}{n_2} \right)^2 \frac{\gamma}{\varrho} \right]^2}, \\
 R(\gamma, \varrho) &\stackrel{\text{def}}{=} \frac{1/\gamma}{1 + \left[\left(\frac{n_1}{n_2} \right)^2 \frac{\gamma}{\varrho} \right]^2} \left[\left(\frac{n_1}{n_2} \right)^2 \left(1 + e^{-2\gamma(r+w)} + 2 \left(\frac{\gamma}{\varrho} \right)^2 \right) \right. \\
 &\quad \left. + \left(\frac{n_1}{n_2} \right)^2 (1 - e^{-2\gamma r}) + \left(\frac{n_2}{n_1} \right)^2 (e^{-2\gamma r} - e^{-2\gamma(r+w)}) \right], \tag{11}
 \end{aligned}$$

respectively, and for $k_0 \stackrel{\text{def}}{=} 2\pi/\lambda$,

$$\begin{aligned}
 \varrho_1 &= \sqrt{k_0^2 n_1^2 - \beta_1^2}, & \varrho_{\text{single}} &= \sqrt{k_0^2 n_1^2 - (\beta_M^{\text{single}})^2}, \\
 \gamma_1 &= \sqrt{\beta_1^2 - k_0^2 n_2^2}, & \gamma_{\text{single}} &= \sqrt{(\beta_M^{\text{single}})^2 - k_0^2 n_2^2}. \tag{12}
 \end{aligned}$$

Defining

$$w_{\text{eff}} = w + Q(\gamma_1, \varrho_1), \quad d_{\text{eff}} = d + Q(\gamma_{\text{single}}, \varrho_{\text{single}}), \tag{13}$$

the coupling coefficients $\kappa_1, t_0, \zeta_1, \varpi_1, \varsigma_1, \chi_1, \vartheta_0$ are given by

$$\begin{aligned}
 \kappa_1 &\stackrel{\text{def}}{=} \frac{\omega\mu_0}{4n_2^2} \int_{|x-w/2-r/2| \leq t/2} \mathcal{H}_1^*(x) \mathcal{H}_0(x) dx \\
 &= \frac{2(n_1/n_2)^2}{n_1^2 - n_2^2} \frac{\varrho_1 \varrho_{\text{single}}}{\sqrt{\beta_1 w_{\text{eff}} \beta_M^{\text{single}} d_{\text{eff}}}} \\
 &\quad \times \frac{\sinh(\gamma_{\text{single}} - \gamma_1)t/2}{(\gamma_{\text{single}} - \gamma_1)} e^{-(\gamma_{\text{single}} + \gamma_1)r/2}, \tag{14}
 \end{aligned}$$

$$\begin{aligned}
 t_0 &\stackrel{\text{def}}{=} \frac{\omega\mu_0}{4n_2^2} \int_{|x-w/2-r/2| \leq t/2} |\mathcal{H}_0(x)|^2 dx \\
 &= \frac{(n_1/n_2)^2}{n_1^2 - n_2^2} \frac{\varrho_{\text{single}}^2}{\beta_M^{\text{single}} d_{\text{eff}}} \frac{\sinh(\gamma_{\text{single}} t)}{\gamma_{\text{single}}} e^{-\gamma_{\text{single}} r}, \\
 \zeta_1 &\stackrel{\text{def}}{=} \frac{\omega\mu_0}{4n_2^2} \int_{|x-w/2-r/2| \leq t/2} |\mathcal{H}_1(x)|^2 dx \\
 &= \frac{(n_1/n_2)^2}{n_1^2 - n_2^2} \frac{\varrho_1^2}{\beta_1 w_{\text{eff}}} \frac{\sinh(\gamma_1 t)}{\gamma_1} e^{-\gamma_1 r}, \tag{15}
 \end{aligned}$$

$$\begin{aligned}
 \varpi_1 &\stackrel{\text{def}}{=} \frac{\omega\mu_0}{4n_1^2} \int_{|x-w/2-r-d/2| \leq d/2} \mathcal{H}_0^*(x) \mathcal{H}_1(x) dx \\
 &= \frac{1}{n_1^2 - n_2^2} \frac{\varrho_1 \varrho_{\text{single}}}{\sqrt{\beta_1 w_{\text{eff}} \beta_M^{\text{single}} d_{\text{eff}}}} \frac{\gamma_1 + \gamma_{\text{single}}}{\gamma_1^2 + \varrho_{\text{single}}^2} e^{-\gamma_1 r}, \\
 \varsigma_1 &\stackrel{\text{def}}{=} \frac{\omega\mu_0}{4n_1^2} \int_{|x| \leq w/2} \mathcal{H}_1^*(x) \mathcal{H}_0(x) dx \\
 &= \frac{1}{n_1^2 - n_2^2} \frac{\varrho_1 \varrho_{\text{single}}}{\sqrt{\beta_1 w_{\text{eff}} \beta_M^{\text{single}} d_{\text{eff}}}} \frac{\gamma_1 + \gamma_{\text{single}}}{\varrho_1^2 + \gamma_{\text{single}}^2} e^{-\gamma_{\text{single}} r}, \tag{16}
 \end{aligned}$$

$$\begin{aligned}
 \chi_1 &\stackrel{\text{def}}{=} \frac{\omega\mu_0}{4n_2^2} \int_{|x+w/2+t_w/2| \leq t_w/2, |x-w/2-r-d-t_d/2| \leq t_d/2} |\mathcal{H}_1(x)|^2 dx \\
 &= \frac{(n_1/n_2)^2}{n_1^2 - n_2^2} \frac{\varrho_1^2}{\beta_1 w_{\text{eff}}} \frac{\sinh(\gamma_1 t_w)}{\gamma_1} e^{-\gamma_1 t_w}, \\
 \vartheta_0 &\stackrel{\text{def}}{=} \frac{\omega\mu_0}{4n_2^2} \int_{|x+w/2+t_w/2| \leq t_w/2, |x-w/2-r-d-t_d/2| \leq t_d/2} |\mathcal{H}_0(x)|^2 dx \\
 &= \frac{(n_1/n_2)^2}{n_1^2 - n_2^2} \frac{\varrho_{\text{single}}^2}{\beta_{\text{single}} d_{\text{eff}}} \frac{\sinh(\gamma_{\text{single}} t_d)}{\gamma_{\text{single}}} e^{-\gamma_{\text{single}} t_d}. \tag{17}
 \end{aligned}$$

4. SOLUTION OF THE COUPLED-MODE EQUATIONS AND GRATINGS' DESIGN

Noticing that Eq. (9) is a set of linear differential equations with coefficients that depend on z , we make the following change of variables to get a set of linear differential equations with constant coefficients:

$$\begin{aligned} A_1^+(z) &= e^{j\Delta\beta_1 z} x_1(z), & A_1^-(z) &= e^{-j\Delta\beta_1 z} x_3(z), \\ C_0^+(z) &= e^{j\Delta\beta_M^{\text{single}} z} x_2(z), & C_0^-(z) &= e^{-j\Delta\beta_M^{\text{single}} z} x_4(z). \end{aligned} \quad (18)$$

Accordingly, we get Eq. (21), which can be written in matrix form as

$$\dot{X} = AX, \quad (19)$$

where

$$\begin{aligned} \dot{X} &\stackrel{\text{def}}{=} \frac{dX}{dz}, & X(z) &= \begin{bmatrix} X_1(z) \\ X_2(z) \end{bmatrix}, \\ X_1(z) &= \begin{bmatrix} x_1(z) \\ x_2(z) \end{bmatrix}, & X_2(z) &= \begin{bmatrix} x_3(z) \\ x_4(z) \end{bmatrix}, \end{aligned} \quad (20)$$

and A is given by Eq. (22). Knowing the initial and final values, as follows:

$$\begin{aligned} \frac{1}{w_{\text{rel}}} \frac{dx_1}{dz} &= -j \left[\left(\frac{\Delta\beta_1}{w_{\text{rel}}} + (b_0\zeta_1 + c_0\chi_1) \right) x_1(z) + (b_0\kappa_1 + 2b_0\varsigma_1)x_2(z) + (b_1\zeta_1 + c_1\chi_1)x_3(z) + b_1\kappa_1 x_4(z) \right], \\ \frac{1}{d_{\text{rel}}} \frac{dx_2}{dz} &= -j \left[(b_0\kappa_1^* + 2b_0\varpi_1)x_1(z) + \left(\frac{\Delta\beta_M^{\text{single}}}{d_{\text{rel}}} + (b_0\iota_0 + c_0\vartheta_0) \right) x_2(z) + b_1\kappa_1^* x_3(z) + (b_1\iota_0 + c_1\vartheta_0)x_4(z) \right], \\ \frac{1}{w_{\text{rel}}} \frac{dx_3}{dz} &= j \left[(b_1^*\zeta_1 + c_1^*\chi_1)x_1(z) + b_1^*\kappa_1 x_2(z) + \left(\frac{\Delta\beta_1}{w_{\text{rel}}} + (b_0\zeta_1 + c_0\chi_1) \right) x_3(z) + (b_0\kappa_1 + 2b_0\varsigma_1)x_4(z) \right], \\ \frac{1}{d_{\text{rel}}} \frac{dx_4}{dz} &= j \left[b_1^*\kappa_1^* x_1(z) + (b_1^*\iota_0 + c_1^*\vartheta_0)x_2(z) + (b_0\kappa_1^* + 2b_0\varpi_1)x_3(z) + \left(\frac{\Delta\beta_M^{\text{single}}}{d_{\text{rel}}} + (b_0\iota_0 + c_0\vartheta_0) \right) x_4(z) \right], \end{aligned} \quad (21)$$

$$A = \begin{bmatrix} -j(\Delta\beta_1 + w_{\text{rel}}(b_0\zeta_1 + c_0\chi_1)) & -jw_{\text{rel}}(b_0\kappa_1 + 2b_0\varsigma_1) & -jw_{\text{rel}}(b_1\zeta_1 + c_1\chi_1) & -jw_{\text{rel}}b_1\kappa_1 \\ -jd_{\text{rel}}(b_0\kappa_1^* + 2b_0\varpi_1) & -j(\Delta\beta_M^{\text{single}} + d_{\text{rel}}(b_0\iota_0 + c_0\vartheta_0)) & -jd_{\text{rel}}b_1\kappa_1^* & -jd_{\text{rel}}(b_1\iota_0 + c_1\vartheta_0) \\ jw_{\text{rel}}(b_1^*\zeta_1 + c_1^*\chi_1) & jw_{\text{rel}}b_1^*\kappa_1 & j(\Delta\beta_1 + w_{\text{rel}}(b_0\zeta_1 + c_0\chi_1)) & jw_{\text{rel}}(b_0\kappa_1 + 2b_0\varsigma_1) \\ jd_{\text{rel}}b_1^*\kappa_1^* & jd_{\text{rel}}(b_1^*\iota_0 + c_1^*\vartheta_0) & jd_{\text{rel}}(b_0\kappa_1^* + 2b_0\varpi_1) & j(\Delta\beta_M^{\text{single}} + d_{\text{rel}}(b_0\iota_0 + c_0\vartheta_0)) \end{bmatrix}, \quad (22)$$

$$X_1(0) = \begin{bmatrix} A_1^+(0) \\ 0 \end{bmatrix}, \quad X_2(L) = \begin{bmatrix} 0 \\ 0 \end{bmatrix}, \quad (23)$$

we get the solution

$$\begin{bmatrix} X_1(L) \\ X_2(0) \end{bmatrix} = \begin{bmatrix} (\Phi_{11}(L) - \Phi_{12}(L)\Phi_{22}^{-1}(L)\Phi_{21}(L))X_1(0) \\ -\Phi_{22}^{-1}(L)\Phi_{21}(L)X_1(0) \end{bmatrix}, \quad (24)$$

where

$$\begin{bmatrix} \Phi_{11}(z) & \Phi_{12}(z) \\ \Phi_{21}(z) & \Phi_{22}(z) \end{bmatrix} = e^{Az}. \quad (25)$$

A. Cost Functions

To minimize the effect of return losses and increase bandwidth, we define the following cost functions:

$$\begin{aligned} f_{\text{cost}}^{(1)}(t_w) &\stackrel{\text{def}}{=} b_0\zeta_1 + c_0\chi_1 \\ &= \left(\frac{n_1}{n_2} \right)^2 \frac{Q_1^2}{\beta_1 w_{\text{eff}}} \left[\frac{\sinh(\gamma_1 t)}{2\gamma_1} e^{-\gamma_1 t} + \frac{D \sinh(\gamma_1 t_w)}{\gamma_1} e^{-\gamma_1 t_w} \right], \end{aligned} \quad (26)$$

$$\begin{aligned} f_{\text{cost}}^{(2)}(t_d) &\stackrel{\text{def}}{=} b_0\iota_0 + c_0\vartheta_0 \\ &= \left(\frac{n_1}{n_2} \right)^2 \frac{Q_{\text{single}}^2}{\beta_M^{\text{single}} d_{\text{eff}}} \left[\frac{\sinh(\gamma_{\text{single}} t)}{2\gamma_{\text{single}}} e^{-\gamma_{\text{single}} t} \right. \\ &\quad \left. + \frac{D \sinh(\gamma_{\text{single}} t_d)}{\gamma_{\text{single}}} e^{-\gamma_{\text{single}} t_d} \right], \end{aligned} \quad (27)$$

$$\begin{aligned} f_{\text{cost}}^{(3)}(t_w, D) &\stackrel{\text{def}}{=} \frac{1}{2} (b_1\zeta_1 + c_1\chi_1 + b_1^*\zeta_1 + c_1^*\chi_1) \\ &= \left(\frac{n_1}{n_2} \right)^2 \frac{Q_1^2}{\beta_1 w_{\text{eff}}} \left[\frac{\sinh(\gamma_1 t)}{\pi\gamma_1} e^{-\gamma_1 t} \right. \\ &\quad \left. + D \text{sinc}(D) \cos\left(\frac{2\pi\alpha}{\Lambda}\right) \frac{\sinh(\gamma_1 t_w)}{\gamma_1} e^{-\gamma_1 t_w} \right], \end{aligned} \quad (28)$$

and

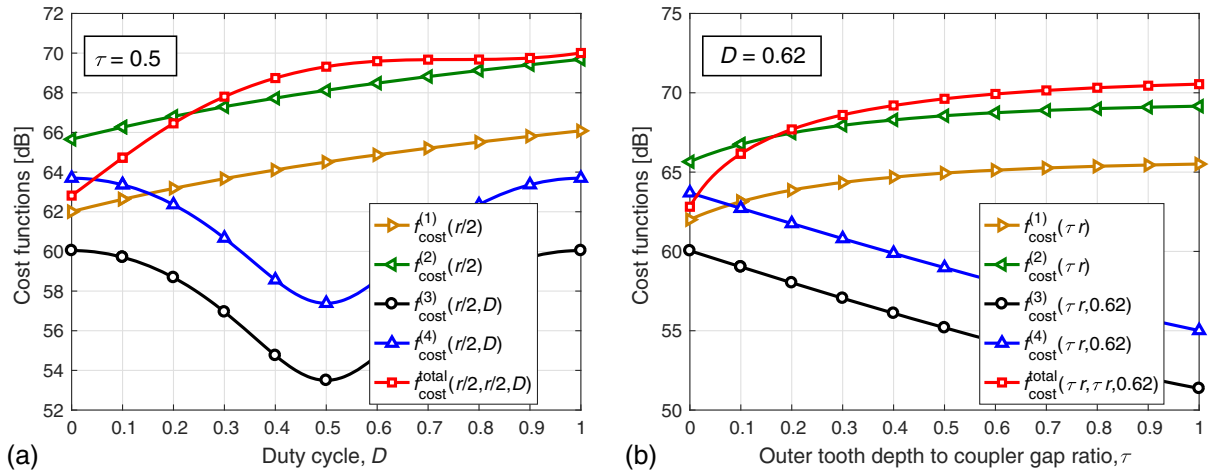


Fig. 2. Cost functions for antireflection gratings versus: (a) duty cycle D with teeth depths of $t_w = t_d = r/2$, (b) teeth-depth-to-coupler-gap ratio τ with a duty cycle of $D = 0.62$.

$$\begin{aligned}
 f_{\text{cost}}^{(4)}(t_d, D) &\stackrel{\text{def}}{=} \frac{1}{2} (b_1 t_0 + c_1 \vartheta_0 + b_1^* t_0 + c_1^* \vartheta_0) \\
 &= \left(\frac{n_1}{n_2} \right)^2 \frac{Q_{\text{single}}^2}{\beta_M^{\text{single}} d_{\text{eff}}} \left[\frac{\sinh(\gamma_{\text{single}} t)}{\pi \gamma_{\text{single}}} e^{-\gamma_{\text{single}} r} \right. \\
 &\quad \left. + D \text{sinc}(D) \cos\left(\frac{2\pi\alpha}{\Lambda}\right) \frac{\sinh(\gamma_{\text{single}} t_d)}{\gamma_{\text{single}}} e^{-\gamma_{\text{single}} t_d} \right]. \quad (29)
 \end{aligned}$$

Minimizing $f_{\text{cost}}^{(3)}$ would reduce the effect of return losses in the multimode waveguide, while minimizing $f_{\text{cost}}^{(4)}$ would reduce the effect of reflection losses in the single-mode waveguide. On the other hand, maximizing both $f_{\text{cost}}^{(1)}$ and $f_{\text{cost}}^{(2)}$ would reduce the dependence of the wavelengths in both multimode and single-mode waveguides, respectively. In turn, this would increase the bandwidth of the device. This leads us to define a combined cost function as

$$\begin{aligned}
 f_{\text{cost}}^{\text{total}}(t_w, t_d, D) &\stackrel{\text{def}}{=} f_{\text{cost}}^{(1)}(t_w) + f_{\text{cost}}^{(2)}(t_d) \\
 &\quad - f_{\text{cost}}^{(3)}(t_w, D) - f_{\text{cost}}^{(4)}(t_d, D). \quad (30)
 \end{aligned}$$

The selection of these functions can be explained by looking carefully at Eq. (9) or Eq. (21). To reduce the effect of return losses in the multimode waveguide, the coefficient of the third term of the first equation in Eq. (21) has to be minimized. Also, the coefficient of the first term of third equation has to be minimized. Accordingly, $f_{\text{cost}}^{(3)}$ is defined as in Eq. (28). Similarly, to reduce the effect of reflection losses in the single-mode waveguide, the coefficient of the fourth term of the second equation in Eq. (21) has to be minimized, and the coefficient of the second term of fourth equation has to be minimized. Accordingly, $f_{\text{cost}}^{(4)}$ is defined as in Eq. (29). On the other hand, looking carefully at the i th coefficient of the i th equation, $i \in \{1, 2, 3, 4\}$, in Eq. (21), one can notice that these coefficients depend on the wavelength through the terms $\Delta\beta_1$ and $\Delta\beta_M^{\text{single}}$. To reduce the dependence of the wavelengths in both waveguides and increase the bandwidth of the device, one would diminish the effect of

these terms. Accordingly, $f_{\text{cost}}^{(1)}$ and $f_{\text{cost}}^{(2)}$ are defined as in Eqs. (26) and (27), respectively.

B. Gratings Design

In this subsection, we determine the duty cycle and teeth depths of the antireflection gratings. We use a BMDM with the following parameters: a coupler gap $r = 140$ nm, a grating period $\Lambda = 282$ nm, a grating teeth depth $t = r$, a coupling length $L = 10.46$ μm , and a taper length $\ell_{\text{taper}} = 216$ nm at port 2. The widths of waveguides are $w = 650$ nm and $d = 287$ nm. These parameters are determined by following the design method described in [25]. To determine the duty cycle we plot in Fig. 2(a) the cost functions versus the duty cycle for antireflection grating teeth depths of $t_w = t_d = r/2$. The figure shows that both $f_{\text{cost}}^{(3)}(t_w, D)$ and $f_{\text{cost}}^{(4)}(t_d, D)$ are minimized at a duty cycle of $D = 0.5$, while both $f_{\text{cost}}^{(1)}(t_w)$ and $f_{\text{cost}}^{(2)}(t_d)$ are maximized at a duty cycle of $D = 1$. On the other hand, the combined cost function is increasing until about $D = 0.62$, after which it remains almost constant around 70 dB.

In addition, we plot in Fig. 2(b) the cost functions versus antireflection grating teeth-depth-to-coupler-gap ratio $\tau = t_w/r = t_d/r$ for a duty cycle of $D = 0.62$. The figure shows that both $f_{\text{cost}}^{(3)}(t_w, D)$ and $f_{\text{cost}}^{(4)}(t_d, D)$ are decreasing functions in τ , while both $f_{\text{cost}}^{(1)}(t_w)$ and $f_{\text{cost}}^{(2)}(t_d)$ are increasing functions. The combined cost function is rapidly increasing until about $\tau = 0.5$, after which it is slowly increasing and is almost constant around 70 dB.

5. NUMERICAL RESULTS AND FDTD SIMULATIONS

In this section, we use 2D FDTD Solutions to simulate the performance of the proposed BMDM-AR with a slab-waveguides coupler. In our simulation, we use the same parameters as given in Subsection 4.B. The simulation results are sets of S -parameters, defined as follows. When exciting input port 1 of the BMDM-AR by TM_1 mode, the corresponding S -parameters are

$$\begin{aligned} S_{11_{M1}} &= \frac{\mathcal{A}_1^-(0)}{\mathcal{A}_1^+(0)}, & S_{21_M} &= \frac{\mathcal{A}_1^+(L + \ell_{\text{taper}})}{\mathcal{A}_1^+(0)}, \\ S_{31_M} &= \frac{\mathcal{C}_0^+(L)}{\mathcal{A}_1^+(0)}, & S_{41_M} &= \frac{\mathcal{C}_0^-(0)}{\mathcal{A}_1^+(0)}. \end{aligned} \quad (31)$$

The notation $M1$ in $S_{11_{M1}}$ indicates that the S -parameter is determined for TM_1 mode at output port 1 of the multimode waveguide, while the notation M in S_{n1_M} , $n \in \{2, 3, 4\}$, indicates that the S -parameter is determined for the fundamental TM mode at output port n of a single-mode waveguide. Similar definitions can be made when exciting the BMDM-AR by TE_m mode, $m \in \{0, 2\}$, as follows:

$$\begin{aligned} S_{11_{E0}} &= \frac{\mathcal{A}_0^-(0)}{\mathcal{A}_m^+(0)}, & S_{11_{E2}} &= \frac{\mathcal{A}_2^-(0)}{\mathcal{A}_m^+(0)}, \\ S_{21_E} &= \frac{\mathcal{A}_2^+(L + \ell_{\text{taper}})}{\mathcal{A}_m^+(0)}, \\ S_{31_E} &= \frac{\mathcal{B}_0^+(L)}{\mathcal{A}_m^+(0)}, & S_{41_E} &= \frac{\mathcal{B}_0^-(0)}{\mathcal{A}_m^+(0)}. \end{aligned} \quad (32)$$

A. BMDM without Antireflection Gratings

Figure 3 shows the simulation results for traditional BMDM without antireflection gratings. Specifically, the resulting S -parameters are plotted versus wavelength in Figs. 3(a)–3(c), when exciting the (de)multiplexer by TE_0 , TM_1 , and TE_2 , respectively. The crosstalks between TE and TM modes are too small to appear in the figures. It is clear that the device has

acceptable values of crosstalks. However, it has high values of both insertion and return losses. For example, when exciting the BMDM by TM_1 mode, the insertion loss is about $S_{31_M} = -3.3$ dB at $\lambda = 1550$ nm. The return loss is as high as $S_{11_{M1}} = -2.5$ dB at $\lambda = 1565$ nm. When exciting the BMDM by TE_2 mode, the insertion and return losses are about $S_{41_E} = -4.5$ dB and $S_{11_{E2}} = -8.8$ dB, respectively, at $\lambda = 1550$ nm.

It is clear that the device bandwidth is limited because of the high return losses. The estimated bandwidths of the device are about 85 nm, 50 nm, and 20 nm, for TE_0 , TE_2 , and TM_1 modes, respectively.

B. BMDM-AR with Antireflection Gratings of 0.5 Duty Cycle

Figure 4 shows the simulation results when placing extra gratings at the outer sides of the waveguides, phase shifted by 180° with respect to the inner side gratings. The gratings' teeth depth at each of the outer sides equals $t_w = t_d = r/2$, and the duty cycle is $D = 0.5$.

The results show that the high return loss of TM_1 mode is reduced. In addition, the bandwidths of both TM_1 and TE_2 are significantly increased. Specifically, when exciting the BMDM-AR by TM_1 mode, the return loss is reduced to about $S_{11_{M1}} = -5.7$ dB at $\lambda = 1550$ nm. The insertion loss is about $S_{31_M} = -2.92$ dB at $\lambda = 1550$ nm, while the crosstalks to other TE modes are negligibly small.

When exciting the BMDM-AR by TE_0 mode, the insertion loss is about $S_{21_E} = -1.68$ dB at $\lambda = 1550$ nm, while the

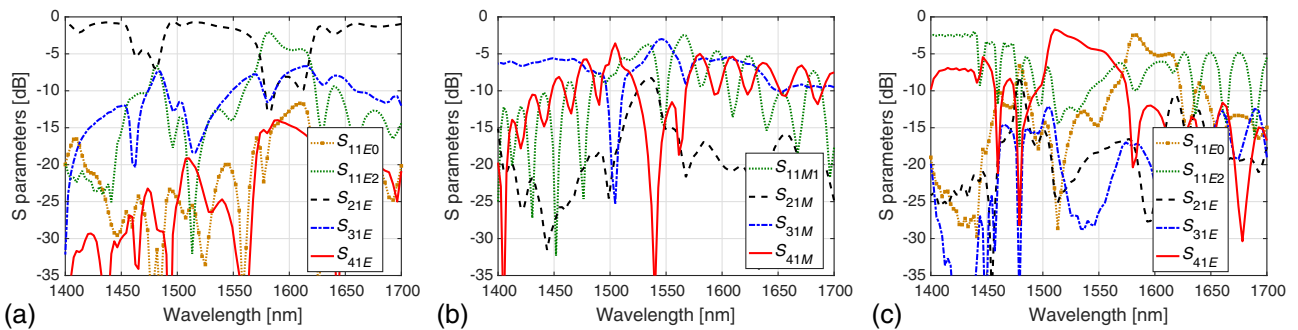


Fig. 3. FDTD simulation of S -parameters versus wavelength of traditional BMDM without antireflection gratings, when excited by (a) TE_0 , (b) TM_1 , and (c) TE_2 modes.

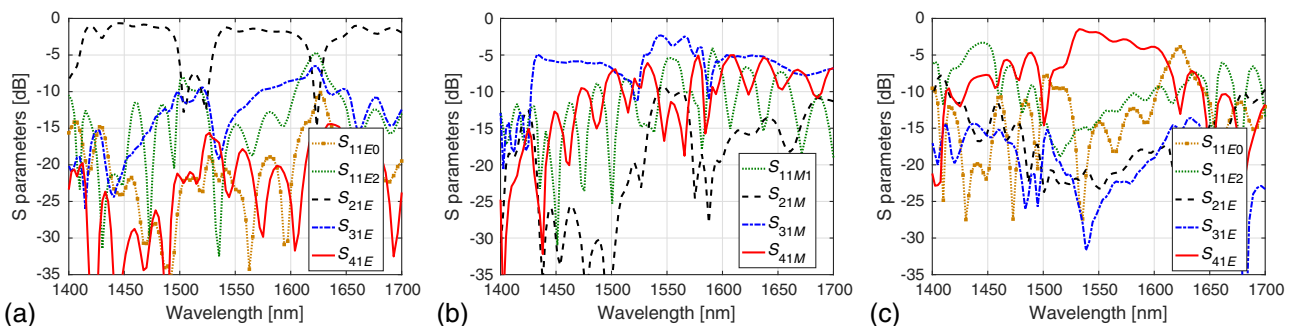


Fig. 4. FDTD simulation of S -parameters versus wavelength of proposed BMDM-AR with antireflection gratings of duty cycle $D = 0.5$ and teeth depths of $t_w = t_d = r/2$, when excited by (a) TE_0 , (b) TM_1 , and (c) TE_2 modes.

return loss and crosstalk are about $S_{11E0} = -23.5$ dB and $S_{41E} = -21$ dB, respectively, at same wavelength. It should be noticed that in this case the insertion loss S_{21E} is increased a bit compared to that in the case without antireflection gratings. Indeed, antireflection gratings would give rise to TE₀-TE₁ mode conversion in the multimode waveguide [32]. This part of TE₁ mode would be coupled into a radiation mode in the taper section and result in some losses.

Finally, when exciting the BMDM-AR by TE₂ mode, the insertion loss is about $S_{41E} = -1.88$ dB at $\lambda = 1550$ nm, while the return loss and crosstalk are about $S_{11E2} = -16.5$ dB and $S_{21E} = -23$ dB, respectively, at the same wavelength. It is also clear that the insertion loss is more flat over a larger bandwidth than that without antireflection gratings.

The estimated bandwidth of the device is about 85 nm for both TE₀ and TE₂ modes, while it is increased to about 40 nm for TM₁ mode.

C. BMDM-AR with Antireflection Gratings of 0.62 Duty Cycle

To reduce the return loss and increase the bandwidth even further, the duty cycle is increased to $D = 0.62$. Figure 5 shows the simulation results for this case.

The results show that the high return loss of TM₁ mode is reduced even further, and its bandwidth is increased. Specifically, when exciting the BMDM-AR by TM₁ mode, the return loss is

significantly reduced to about $S_{11M1} = -15.5$ dB at $\lambda = 1550$ nm, and the insertion loss is significantly improved to about $S_{31M} = -1.88$ dB at the same wavelength.

When exciting the BMDM-AR by TE₀ mode, the insertion loss is about $S_{21E} = -1.33$ dB at $\lambda = 1550$ nm, while the return loss and crosstalk are about $S_{11E0} = -22$ dB and $S_{41E} = -21$ dB, respectively, at the same wavelength.

Finally, when exciting the BMDM-AR by TE₂ mode, the insertion loss is about $S_{41E} = -1.91$ dB at $\lambda = 1550$ nm, while the return loss and crosstalk are about $S_{11E2} = -16$ dB and $S_{21E} = -19$ dB, respectively, at the same wavelength. Also, the insertion loss is about $S_{41E} = -1.33$ dB at $\lambda = 1543$ nm.

In addition, the estimated bandwidth of the device is increased to about 45 nm for TM₁ mode, while it is about 85 nm for both TE₀ and TE₂ modes.

D. Analytical Results

In this subsection, we compare our analytical results, as given in Section 4, with that of the simulations. In Fig. 6, we plot the S-parameters as obtained from the analytical equations when exciting input port 1 of the BMDM-AR by TM₁ mode. Both duty cycles of $D = 0.5$ and $D = 0.62$ are considered. The figures show general consistency with the corresponding simulation figures as given in Figs. 4(b) and 5(b). Of course, some discrepancies exist due to the approximations and ideal material used in the analysis. We have the following remarks.

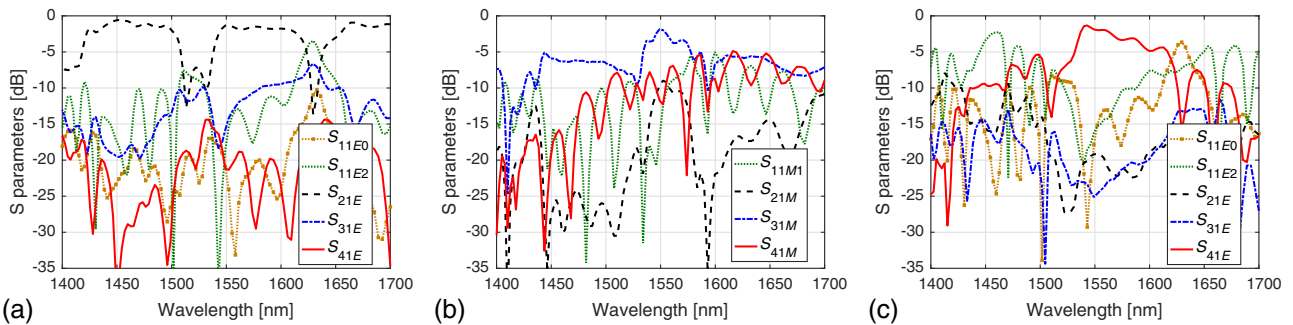


Fig. 5. FDTD simulation of S-parameters versus wavelength of proposed BMDM-AR with antireflection gratings of duty cycle $D = 0.62$ and teeth depths of $t_w = t_d = r/2$, when excited by (a) TE₀, (b) TM₁, and (c) TE₂ modes.

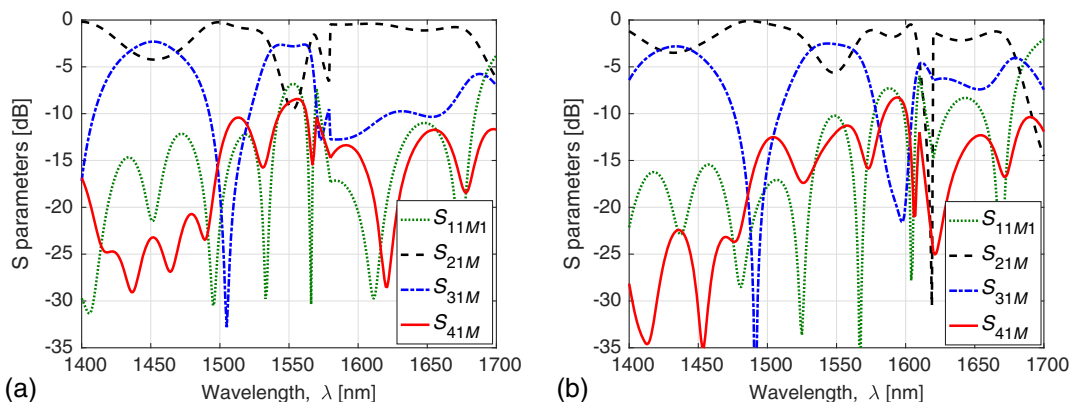


Fig. 6. Analytical S-parameters versus wavelength of proposed BMDM-AR with antireflection gratings of teeth depths of $t_w = t_d = r/2$, when excited by TM₁ for a duty cycle of (a) $D = 0.5$ and (b) $D = 0.62$.

The high return loss of TM_1 mode ($S_{11,M1}$) is significantly reduced when using a duty cycle of $D = 0.62$. In addition, the device bandwidth is increased at this duty cycle. One more remark is the crosstalk to port 2 ($S_{21,M}$) is higher in the analytical results than that in the simulations. The reason is that the analytical results are obtained without a taper at the output of the multimode waveguide, while the simulations have been done with a taper. Indeed, the taper helps in radiating away the crosstalk due to first-order mode.

6. CONCLUSIONS

The impact of return losses on the performance of BMDMs have been studied, and antireflection gratings have been designed to reduce their effect. Approximate analytical expressions that obtain the optimal design parameters have been derived based on the perturbative coupled-mode theory. Both duty cycle and teeth depths of the antireflection gratings have been determined based on optimizing a cost function. In addition, FDTD simulation of the proposed device has been performed, and its S -parameters have been obtained and presented for different design parameters. Our results reveal that for antireflection gratings with a duty cycle of 0.62, the insertion losses, return losses, and crosstalks are significantly reduced. In addition, the estimated bandwidth of the device is significantly increased to about 45 nm for TM_1 mode, while it is about 85 nm for both TE_0 and TE_2 modes.

REFERENCES

1. D. J. Richardson, J. M. Fini, and L. E. Nelson, "Space-division multiplexing in optical fibres," *Nat. Photonics* **7**, 354–362 (2013).
2. S. Berdagué and P. Facq, "Mode division multiplexing in optical fibers," *Appl. Opt.* **21**, 1950–1955 (1982).
3. J. Wang, P. Chen, S. Chen, Y. Shi, and D. Dai, "Improved 8-channel silicon mode demultiplexer with grating polarizers," *Opt. Express* **22**, 12799–12807 (2014).
4. A. Grieco, G. Porter, and Y. Fainman, "Integrated space-division multiplexer for application to data center networks," *IEEE J. Sel. Top. Quantum Electron.* **22**, 1–6 (2016).
5. D. Dai and J. E. Bowers, "Silicon-based on-chip multiplexing technologies and devices for peta-bit optical interconnects," *Nanophotonics* **3**, 283–311 (2014).
6. D. Dai and S. Wang, "Silicon-based reconfigurable optical add-drop multiplexer for hybrid MDM-WDM systems," in *Proceedings of the IEEE/OSA Optical Fiber Communication Conference (OFC)* (Optical Society of America, 2017), paper Tu2C.1.
7. T. Uematsu, Y. Ishizaka, Y. Kawaguchi, K. Saitoh, and M. Koshiba, "Design of a compact two-mode multi/demultiplexer consisting of multimode interference waveguides and a wavelength-insensitive phase shifter for mode-division multiplexing transmission," *J. Lightwave Technol.* **30**, 2421–2426 (2012).
8. Y. Ding, J. Xu, F. D. Ros, B. Huang, H. Ou, and C. Peucheret, "On-chip two-mode division multiplexing using tapered directional coupler-based mode multiplexer and demultiplexer," *Opt. Express* **21**, 10376–10382 (2013).
9. D. Dai, J. Wang, and Y. Shi, "Silicon mode (de)multiplexer enabling high capacity photonic networks-on-chip with a single-wavelength-carrier light," *Opt. Lett.* **38**, 1422–1424 (2013).
10. H. Qiu, H. Yu, T. Hu, G. Jiang, H. Shao, P. Yu, J. Yang, and X. Jiang, "Silicon mode multi/demultiplexer based on multimode grating-assisted couplers," *Opt. Express* **21**, 17904–17911 (2013).
11. W. Chen, P. Wang, and J. Yang, "Mode multi/demultiplexer based on cascaded asymmetric Y-junctions," *Opt. Express* **21**, 25113–25119 (2013).
12. J. B. Driscoll, R. R. Grote, B. Souhan, J. I. Dadap, M. Lu, and R. M. Osgood, "Asymmetric Y junctions in silicon waveguides for on-chip mode-division multiplexing," *Opt. Lett.* **38**, 1854–1856 (2013).
13. J. Xing, Z. Li, X. Xiao, J. Yu, and Y. Yu, "Two-mode multiplexer and demultiplexer based on adiabatic couplers," *Opt. Lett.* **38**, 3468–3470 (2013).
14. L.-W. Luo, N. Ophir, C. P. Chen, L. H. Gabrielli, C. B. Poitras, K. Bergmen, and M. Lipson, "WDM-compatible mode-division multiplexing on a silicon chip," *Nat. Commun.* **5**, 3069 (2014).
15. J. Wang, S. He, and D. Dai, "On-chip silicon 8-channel hybrid (de)multiplexer enabling simultaneous mode- and polarization-division-multiplexing," *Laser Photon. Rev.* **8**, L18–L22 (2014).
16. B. A. Dorin and W. N. Ye, "Two-mode division multiplexing in a silicon-on-insulator ring resonator," *Opt. Express* **22**, 4547–4558 (2014).
17. D. Dai, "Multimode optical waveguide enabling microbends with low inter-mode crosstalk for mode-multiplexed optical interconnects," *Opt. Express* **22**, 27524–27534 (2014).
18. N. Hanzawa, K. Saitoh, T. Sakamoto, T. Matsui, K. Tsujikawa, M. Koshiba, and F. Yamamoto, "Mode multi/demultiplexing with parallel waveguide for mode division multiplexed transmission," *Opt. Express* **22**, 29321–29330 (2014).
19. H. Chen, R. van Uden, C. Okonkwo, and T. Koonen, "Compact spatial multiplexers for mode division multiplexing," *Opt. Express* **22**, 31582–31594 (2014).
20. M. Yin, Q. Deng, Y. Li, X. Wang, and H. Li, "Compact and broadband mode multiplexer and demultiplexer based on asymmetric plasmonic-dielectric coupling," *Appl. Opt.* **53**, 6175–6180 (2014).
21. C. Gui, Y. Gao, Z. Zhang, and J. Wang, "On-chip silicon two-mode (de)multiplexer for OFDM/OQAM data transmission based on grating-assisted coupler," *IEEE Photon. J.* **7**, 7905807 (2015).
22. C. Williams, B. Banan, G. Cowan, and O. Liboiron-Ladouceur, "Source-synchronous optical link using mode-division multiplexing," in *IEEE 12th International Conference on Group IV Photonics (GFP)* (2015), pp. 110–111.
23. B. Stern, X. Zhu, C. P. Chen, L. D. Tzuang, J. Cardenas, K. Bergman, and M. Lipson, "On-chip mode-division multiplexing switch," *Optica* **2**, 530–535 (2015).
24. T. Mulugeta and M. Rasras, "Silicon hybrid (de)multiplexer enabling simultaneous mode and wavelength-division multiplexing," *Opt. Express* **23**, 943–949 (2015).
25. H. M. H. Shalaby, "Bi-directional coupler as a mode-division multiplexer/demultiplexer," *J. Lightwave Technol.* **34**, 3633–3640 (2016).
26. O. M. Nawwar, H. M. H. Shalaby, and R. K. Pokharel, "Compact mode-division de(multiplexer) with anti-reflection grating for optical interconnects," in *Proceedings of the Asia Communications and Photonics Conference (ACP)* (Optical Society of America, 2016), paper AF1G.7.
27. J. A. H. Odoeze, O. M. Nawwar, and H. M. H. Shalaby, "J-rib waveguide as a mode-division demultiplexer," in *Proceedings of the Asia Communications and Photonics Conference (ACP)* (Optical Society of America, 2016), paper AF1G.6.
28. H. Xu and Y. Shi, "Ultra-broadband 16-channel mode division (de) multiplexer utilizing densely packed bent waveguide arrays," *Opt. Lett.* **41**, 4815–4818 (2016).
29. O. M. Nawwar, H. M. H. Shalaby, and R. K. Pokharel, "Design and fabrication of a bi-directional mode-division multiplexer (BMDM) for optical interconnects," in *Proceedings of the IEEE Photonics Conference (IPC)* (2017).
30. W. Shi, M. Greenberg, X. Wang, Y. Wang, C. Lin, N. A. F. Jaeger, and L. Chrostowski, "Single-band add-drop filters using anti-reflection, contra-directional couplers," in *The 9th International Conference on Group IV Photonics (GFP)* (2012), pp. 21–23.
31. W. Shi, H. Yun, C. Lin, M. Greenberg, X. Wang, Y. Wang, S. T. Fard, J. Flueckiger, N. A. F. Jaeger, and L. Chrostowski, "Ultra-compact, flat-top demultiplexer using anti-reflection contra-directional couplers for CWDM networks on silicon," *Opt. Express* **21**, 6733–6738 (2013).
32. A. Mohanty, M. Zhang, A. Dutt, S. Ramelow, P. Nussenzweig, and M. Lipson, "Quantum interference between transverse spatial waveguide modes," *Nat. Commun.* **8**, 14010 (2017).